PCCP

Accepted Manuscript




ROYAL SOCIETY OF CHEMISTRY

www.rsc.org/pccp

PCCP

RSCPublishing

ARTICLE

# Kink Energy and Kink Dipole Moment on Vicinal Au(001) in Halide Electrolytes

Cite this: DOI: 10.1039/x0xx00000x

M. Al-Shakran,[a] G. Beltramo[b] and M. Giesen[c*],

Received 00th February 2014,
Accepted 00th January 2014

DOI: 10.1039/x0xx00000x

www.rsc.org/

Using electrochemical scanning tunnelling microscopy, we measured the potential-dependent kink energy and the corresponding dipole moments for kinks at step edges on vicinal Au(001) surfaces in chloride and bromide containing electrolyte. Combining the results for the potential dependence of the kink energy with impedance spectroscopy data for the surface charge, we can directly deduce the dipole moment of kinks at the Au steps with co-adsorbed $Cl^-$, respectively $Br^-$. We find $\mu^{Cl} = (6.0 \pm 0.7) \times 10^{-3}\ e$Å and $\mu^{Br} = (10.1 \pm 0.6) \times 10^{-3}\ e$Å.

## Introduction

The investigation of transport processes at electrode surfaces in electrochemical environment has attracted scientific interest for a couple of years due to their relevance in electrochemical processes such as equilibrium and non-equilibrium dynamics[1] corrosion[2, 3] and catalysis[4] and also in applied research such as battery-related transport phenomena[5]. Recently it has been demonstrated that all migration processes have an exponential dependence on the electrode potential[6-8]. In these reports, it was shown that defects at charged surfaces carry a dipole moment that contributes linearly to the energy of the defect in the electric field of the double layer and consequently, adds an exponential dependence of the transport rates on the electrode potential to Boltzmann terms for activated transport processes or defect formation. This concept has meanwhile been confirmed in further experimental studies in electrolyte[9, 10].

In order to understand the details of transport processes in electrochemical systems it is therefore of enormous importance to know the dipole moments of migrating defects. Unfortunately, experimental as well as theoretical values are still scarce: Theoretical studies by Müller and Ibach considered the dipole moment of free adatoms on Au, Ag and Cu surfaces in vacuum using cluster calculations[8]. The data as obtained by Müller et al. fit nicely to experimental data on the decay of islands on Au(001)[6]. Pötting et al. employed density functional theory (DFT) methods to calculate the dipole moments of transition states for a large number of diffusion paths on silver surfaces[11]. In further studies by Cockayne and Burton, DFT calculations were used to determine the dipole moment of Pb-O vacancy pairs in $PbTiO_3$ [12]. Step dipole moments on metal electrodes have been measured using impedance spectroscopy[13, 14]. Recently, the dipole moment of adsorbates on metal electrodes have been determined experimentally by Magnussen and coworkers[10, 15].

Experimental data on the dipole moment of kinks at steps that are preferred binding sites and therefore serve as sinks and sources in growth and degradation phenomena are not available to date.

The aim of this paper is to fill this gap: We present an experimental method to determine the dipole moment of kinks at steps, using a combination of potential dependent measurements of step fluctuations and experimental data on the surface charge. The method is demonstrated for the particular system of stepped Au(001) electrodes in dilute halide solutions with specific adsorption present. The method to measure the kink dipole moment as such, however, is not restricted to systems with specifically adsorbed anions, but rather can be applied to electrolyte interfaces in general.

## Experimental

### STM measurements

Experimental data was acquired using the electrochemical version of the Topometrix TMX 2010 Discoverer STM. Our instrument is modified to enable temperature variable STM recording as described earlier [16, 17]. The results reported here, however, is data for 293 K exclusively. Tip and sample potential are independently controlled via a bipotentiostat.

As samples we used Au ($11n$) singly crystal electrodes ($n$ = 17 and 29), vicinal to Au(001) with ⟨110⟩-oriented steps and (001) terraces of mean width $\frac{n}{2}a_\perp$ ($a_\perp$ the nearest-neighbor distance perpendicular to ⟨110⟩). These surfaces have a small miscut angle (4.8° and 2.8°, respectively) to the (001) plane and hence a high density of parallel steps and are suitable electrodes to study step and kink properties with a large statistical database. For the data presented here, we typically analyzed a total step length of several µm for a distinct electrode potential. The electrodes were spark eroded from a single crystal rod, oriented by diffractometry and polished to the desired orientation to within 0.1°, which is the accuracy of high-quality single crystals. The accuracy is limited by the mosaic structure of the crystal.

Prior to experiment, the Au(001) electrodes were heated in a hydrogen atmosphere and then flame annealed for 5 min to about 900°C. The temperature was visually controlled by the color of the annealed crystal. After thoroughly rinsing the cell with Milli-Q water, the crystals were mounted in the electrochemical STM cell connected to a bipotentiostat. The crystal surface was then brought in contact with the electrolyte

under potential control. This was visually checked prior to STM experiment by the presence of the well-ordered quasi-hexagonal reconstruction of the clean Au(001) surface [18].

As electrolytes, we used suprapure $HClO_4$, HCl and KBr (all Merck) and Milli-Q water from a Millipore Elix 3 and A10 Gradient system (18.2 MΩ $cm^{-1}$; organic contents <3 ppb). The STM measurements were performed in 0.1 M $HClO_4$ + 1mM HCl, respectively 0.1 M $HClO_4$ + 1mM KBr.

The tunnelling tips used in the experiments were etched from tungsten wires following standard procedures [19-21] and coated with polyethylene to avoid Faraday currents at the foremost part of the tip. We used a tunnelling current of 2 nA. The typical time per image was 40 s and the STM images were recorded with a 400×400 pixel resolution in the constant current mode.

High-purity, flame-annealed Pt wires (Goodfellow, 99.999%) served as counter and quasi-reference electrodes. In the following, the electrode potentials of the metal sample, however, are given with respect to the saturated calomel electrode (SCE). As a caveat we emphasize that the electrode potentials denoted here are the nominal values given by the bipotentiostat. Since Pt is a quasi-reference, non-ideally polarizable electrode, we cannot exclude that the potential values as denoted here might deviate from the real potential by about 50 mV due to possible shifts in the open circuit potential of the Pt wire during measurement.

Depending on the chosen electrode potential, good experimental conditions lasted for 30 min up to 2 h. Then, generally, contamination of the electrolyte in the open STM cell became visible and the measurements were terminated.

Step profiles in STM images were analyzed using a special computer code that determines the maximum slope in the grey scale in an individual scan line of the STM image. To account for possible drift in the STM image we analyzed exclusively step pairs[22], a procedure that proved successful in a large number of studies of step fluctuations in vacuum as well as in electrolyte (for a review see [1]).

**Surface charge measurements**

Capacitance curves were recorded using a Zahner IM5 impedance potentiostat. As electrodes we used flat Au(001) bead-type single crystals prepared according to the Clavilier method [23]. Further preparation of the electrodes prior to experiments followed the same procedure as that for the STM samples described before.

The crystal surface was brought in contact with the electrolyte under potential control at values well below the potential of zero charge (pzc). The contact between the electrode surface and the solution was made by means of the hanging meniscus method[24]. A saturated calomel electrode served as reference electrodes and a platinum foil as counter electrode.

The capacity curves were recorded using a frequency of 20 Hz and amplitude of 5 mV. Data was obtained in the direction of negative sweeps exclusively, i.e. the capacity data is that of the unreconstructed flat Au(001) electrode.

We used electrolytes 9 mM $KClO_4$ + 1 mM KCl and 9 mM $KClO_4$ + 1 mM KBr made from suprapure KCl, KBr and from $KClO_4$ twice recrystallized (all Merck) and Milli-Q water as before. The electrolytes differ from those used in STM experiments: First, the total amount of anions did not exceed 10 mM. Under this condition, the pzc can be determined via the minimum in the differential capacity[25] dominated by the Gouy-Chapman contribution in this case. Second, for the analysis of the surface charge density the capacity curves must be measured at low potentials. For the given system, one would have to measure at potentials negative of the hydrogen evolution onset. The use of $KClO_4$ rather than $HClO_4$ shifts the onset of the hydrogen evolution to lower potentials and allows the measurement of the capacity at sufficiently low potentials. Hence, for the system considered in this work, the use of $KClO_4$ for the capacity curve is preferred over the use of $HClO_4$. Although the two electrolytes differ in pH, the shift in pzc is negligibly small.

In order to check for a possible influence of the different electrolytes on our results, we additionally measured cyclic voltamograms (CV) in 9 mM $XClO_4$ + 1 mM $XCl$ ($X$ = H or K) and in 9 mM $XClO_4$ ($X$ = H or K) + 1 mM KBr with a rate of 10 mV/s. The CVs in $HClO_4$ and $KClO_4$ are almost identical, safe for the shift of the onset potential of hydrogen evolution at low potentials and of oxygen evolution at high potentials (data not shown here).

For all electrolytes we used, in STM experiments, CV and capacity studies, the important content of the halides, $Cl^-$ and $Br^-$, however, is identical.

The capacity curves were determined using various models for the interface capacity. As was demonstrated in more detail for Ag(111) electrodes in dilute halide containing electrolytes, the chosen model has no significant influence on the capacity curves as long as the potential is well below the range where ordered halide adlayers are formed [26].

## Theory of step fluctuations

Experimental and theoretical data on step fluctuations have been widely discussed in literature throughout the last two decades. Therefore, we refer for details to review articles [1, 27]. As a brief summary, we recall the basic equation for the spatial correlation function $G(y)$ used to determine the kink energy, valid under nearest-neighbor conditions:

$$G(y) = \langle (x(y) - x(y_0))^2 \rangle \approx \frac{2a_1^2}{a_\parallel} e^{-\varepsilon/kT} |y - y_0| \qquad (1)$$

Here, $a_\parallel$, $a_\perp$ are the nearest-neighbor atomic distances parallel and perpendicular to the dense atomic direction ($\langle 110 \rangle$ for *fcc* and $a_\parallel = a_\perp$). $\varepsilon$ is the kink formation energy. The spatial variables $x$ and $y$ denote the directions parallel, respectively perpendicular to the mean step orientation. The reference coordinate $y_0$ may be chosen freely. That is, measuring the correlation function $G(y)$ yields a linear function in the distance $|y - y_0|$. From the slope one determines directly the kink formation energy.

Recently we showed, that defect migration and formation energies depend on electrode potential $\phi$ in electrochemical systems and are directly related to the dipole moment $\mu$ of the defect [6-8]. In the case of kinks we find for the kink energy $\varepsilon$ (with $\varepsilon_0$ the vacuum permittivity):

$$\varepsilon(\phi) = \varepsilon(\phi_{pzc}) - \frac{\mu}{\varepsilon_0}\sigma(\phi) \qquad (2)$$

As was reported in an earlier work[6], eq. (2) is a linear expansion of the kink energy around pzc. The first term $\varepsilon(\phi_{pzc})$ is the kink energy at pzc of the electrode surface with kink defects. $\phi_{pzc}$ slightly differs from that of defect-free surfaces due to the change in work function[6, 25]. The second term describes the change in work function due to the presence of a (kink) defect. Hence, the second term directly relates the dipole moment to the surface charge density. Higher order terms in eq. (2) are proportional to $\sigma^2$. Measurable surface



 

diffusion processes on Au(001) involve very small equilibrium defect concentrations (~ $10^{-6}$ per surface atom). Therefore, higher order terms do not considerably contribute to eq. (2) and are neglected here. Employing eqs. (1) and (2) one can then directly measure the dipole moment of kinks at steps on metal electrodes in electrolyte.

## Results and discussion

Fig. 1 shows STM images of various vicinal Au(11*n*) electrodes in $Cl^-$ and $Br^-$-containing solutions at different potentials. At high potentials, the surface is unreconstructed and the mobility of the steps may become quite large.

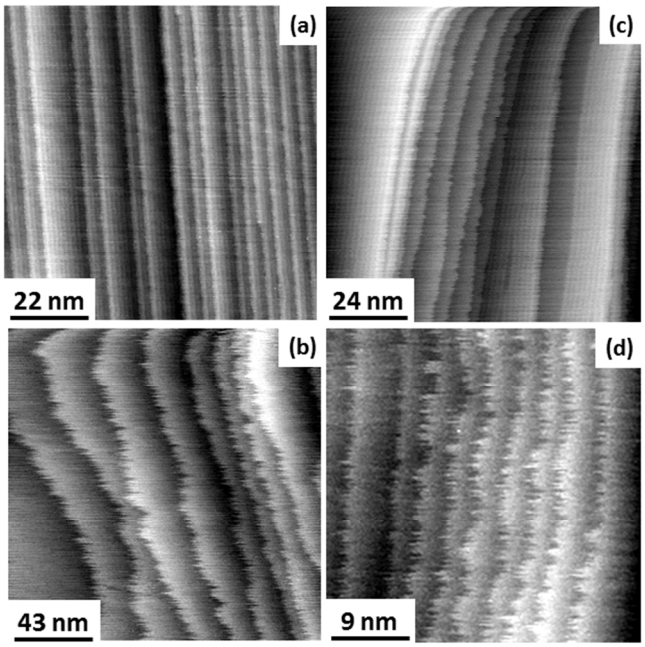


Fig. 1: STM images of Au electrodes in 0.1 M $HClO_4$ + 1 mM HCl (a) (1 1 *29*) at -0.17 V SCE, (b) (1 1 *17*) at +0.45 V SCE and in 0.1 M $HClO_4$ +1 mM KBr (c) (1 1 *29*) at -0.25 V SCE, (d) (1 1 *29*) at +0.31 V SCE.

At low potentials, large terraces are reconstructed. Smaller terraces in regions of high step density remain unreconstructed (Fig. 1(c)). This observation is in accordance to previous data for Au(11*n*) in sulfuric acid[28]. The fact that smaller terraces remain unreconstructed offers the opportunity to measure step fluctuations for the unreconstructed (1×1)-surface even at low potentials. Therefore, the data for step fluctuations and the kink energy in the potential range between –0.25 and +0.55 V SCE as presented in this work is for the unreconstructed Au(001) surface exclusively.

Cyclic voltamograms and surface charge density vs. potential plots are presented in Fig. 2 for $Cl^-$- and $Br^-$- containing solutions as solid and dot-dashed curves, respectively. For comparison, we have plotted the data for the bare surface (without specifically adsorbing halides in the solution) as dotted line. As expected, the surface charge density increases with potential and is the larger the higher the adsorption strength of the anion.

As was demonstrated in [29], capacitance curves on flat Au(001) in pure perchloric acid reveal only minor shifts compared to the respective capacitance of stepped Au(11*n*). Since we deal with electrolytes where the anion strongly specifically adsorbs to the Au electrode we expect no considerable influence of the step density on the surface charge density. We therefore conclude that the experimental results for the surface charge density obtained from flat Au(001) is appropriate to determine the kink dipole moment from step fluctuation data as measured on stepped Au electrodes.

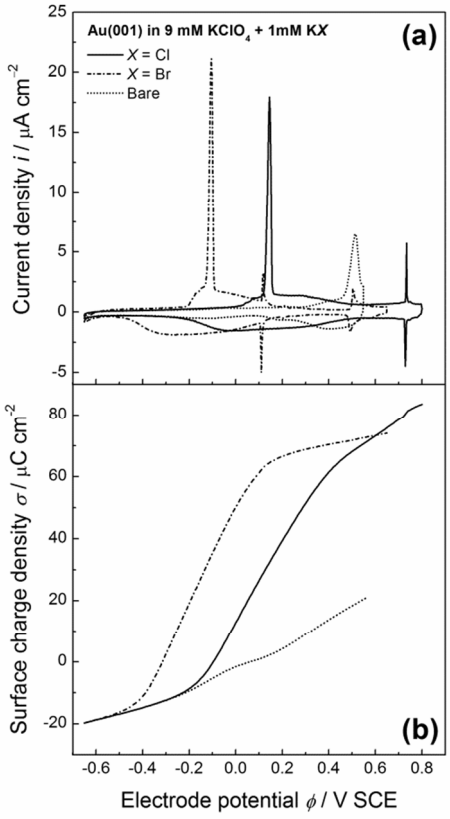


Fig. 2: Cyclic voltamograms (a) and surface charge density vs. potential plots (b) for nominally flat Au(001) electrodes in 9 mM $KClO_4$ + 1mM *X*, *X* = KCl (solid) and *X* = KBr (dot-dashed). For comparison, data for Au(001) in pure 10 mM $KClO_4$ is plotted as dotted lines ("Bare") in both view graphs.

Fig. 3 shows two examples of $G(y)$ as measured for $Cl^-$ and $Br^-$ containing electrolytes at different electrode potentials. For long distances $|y - y_0|$, $G(y)$ is linear. For short distances, the correlation function is obviously curved. This curvature is due to the remaining time contribution to the correlation function. The time contribution originates from the finite scanning speed of the STM tip compared to kink diffusion on the surface. The fast kink movement becomes obvious in the frizzy appearance of the steps[30, 31] in the STM images in Fig. 1, in particular at high potentials where diffusion is fast. The time contribution in STM images and to the spatial correlation function has been extensively considered in [1, 22, 30] and is not further discussed here. We emphasize though that $G(y)$ as plotted in Fig. 3 must undergo careful inspection prior to evaluating the slope and the kink energy. In the studies reported here, we have analyzed

$G(y)$ only in the range of large distances $|y - y_0|$ where the correlation function is linear (solid lines in Fig. 3 are linear fits to $G(y)$ as used for further analysis). From those linear fits one then directly (eq. (1)) obtains the kink energy (Fig. 4). The kink energies for the two electrolytes fall apparently on the same line when plotted vs. electrode potential (Fig. 4(a)). However, plotted vs. surface charge density, the kink energy data obtained in the two electrolytes fall on different curves with apparently different slopes (Fig. 4(b)). According to eq. (2) the kink dipole moment is determined from the slopes of the linear fits in Fig. 4(b) (solid lines). We find

$$\mu^{Cl} = (6.0 \pm 0.7) \times 10^{-3}\, e\text{Å}$$
$$\mu^{Br} = (10.1 \pm 0.6) \times 10^{-3}\, e\text{Å} \qquad (3)$$

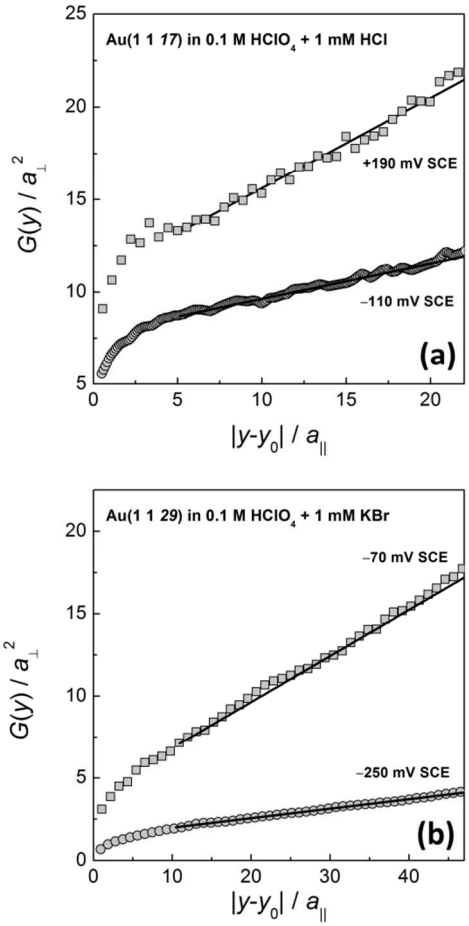


Fig. 3: Spatial correlation function *G(y)* (eq. (1)) for (a) $Cl^-$- and (b) $Br^-$-containing electrolyte at different potentials. Solid lines are linear fits to the curves in the range of large distances (see text for further discussion).

Experimental studies of the kink energy on Au(001) electrodes have been published previously for $H_2SO_4$ and HCl solutions [32-34]. There, kink energies were determined from the curvature of island edges rather than by the analysis of the step correlation function. Fig. 5 shows the previous data (open symbols) [32-34] in comparison with the new data reported here (grey symbols).

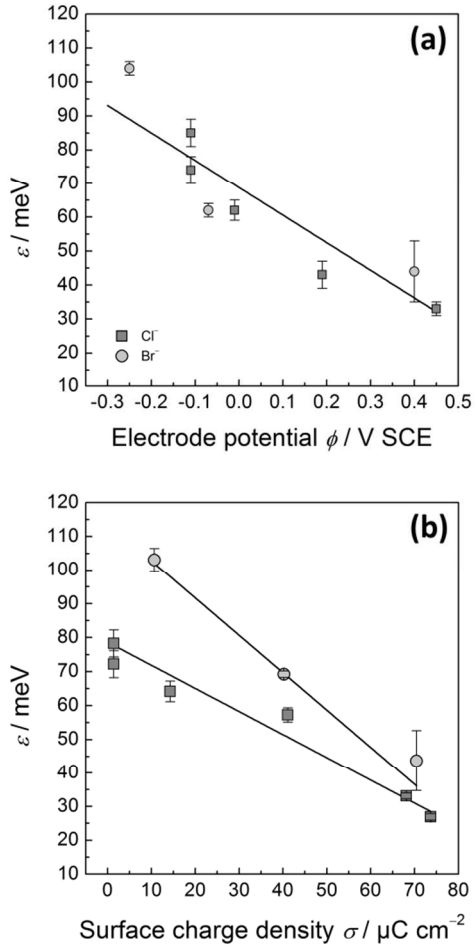


Fig. 4: (a) Kink energy as determined from experimental data for G(y) (eq. (1)) similar to those presented in Fig. 3 for $Cl^-$- (dark grey squares) and $Br^-$- (light grey circles) containing electrolyte vs. electrode potential. (b) The same data plotted vs. surface charge density taken from Fig. 2(b). Solid lines are linear fits to the data (see text for further discussion). Error bars are determined as the standard deviation from the mean for independent measurements at the same electrode potential.

The data for sulfuric acid (open circles)[32, 34] is in excellent agreement with the results we obtained for $Cl^-$ (grey squares) and $Br^-$ (grey circles). The previous data for HCl electrolyte[33], however, seem to strongly deviate from the results reported here. The reason for this deviation is not fully clear. We assume though that the deviation is typical for island perimeter curvature analysis in cases of limited data base: The curvature is determined by calculating the second derivative of the perimeter radius with respect to the polar angle. Hence, low, nevertheless obvious noise in the island perimeter may lead to larger errors in the curvature. These uncertainties are reflected by the relatively large error bars of the previous data in HCl solution (open triangles in Fig. 5). In ultra-high vacuum experiments where the statistical data base is generally much higher than in electrochemical studies, the noise in the perimeter of the island equilibrium shape is negligibly low. Here, the curvature analysis is a very reliable tool to measure the kink energy[35]. In electrochemical studies, however, statistical data base is generally lower due to finite time where

the electrolyte remains clean in the open STM cell. Here, the curvature analysis seems not to be an appropriate tool to obtain exact values for the kink energy, merely an order of magnitude can be determined. We conclude therefore, that the more direct method of measuring spatial step fluctuations is superior to obtain precise values of the kink energy in electrolyte.

Several years ago, we measured a kink energy of 0.074 eV on Au(111) in 0.5 mM HCl at –0.1 V SCE using spatial correlation functions [36]. This value is in excellent agreement with our data for Au(001) in HCl we report here. Effective medium calculations of kink energies on Au(001) and (111) surfaces in vacuum yield values of comparable size [37]. This means that at low potentials where the specific adsorption of halide anions is low, the kink energy in electrolyte is comparable to that in vacuum.

Theoretical values of kink energies in electrolyte were published by Pötting et al. for Ag(100)[11]. Using the embedded atom method, these authors calculated the kink energy as a function of the double-layer field. They showed that the kink energy increases with decreasing electric field (i.e. with decreasing potential) in accordance with our results for Au(001). Furthermore, their kink energy of 0.095 eV for a double-layer field of $1 \times 10^{10}$ V/m is of comparable order of magnitude to our findings on Au(001).

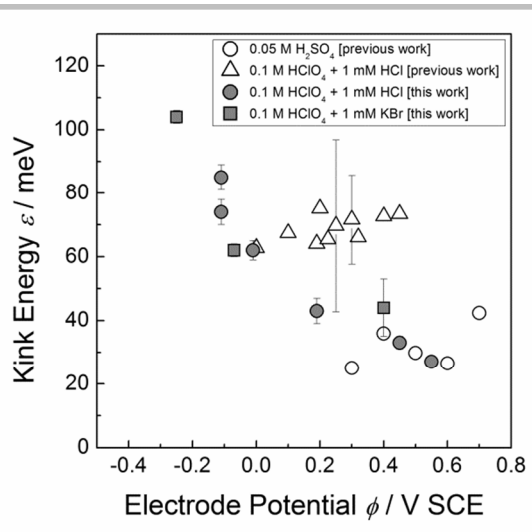


Fig. 5: Comparison of experimentally determined values for the kink energy on Au(100) as obtained previously from the analysis of the island edge curvature [32, 34] (open symbols) with the data as measured in this work from the analysis of the spatial correlation function (grey symbols). See text for discussion.

Our data for the kink dipole moment determined from the step correlation function as reported here may be compared with previous data on defect dipole moments available so far: Several years ago our group presented experimental data on step dipole moments on vicinal Au(11$n$) and Ag(11$n$) electrodes in various electrolytes [13, 14]. We found $\mu_{step}^{SO_4^{2-}} = (6.8 \pm 0.8)\ 10^{-3} e$Å, $\mu_{step}^{ClO_4^-} = (5.2 \pm 0.4)\ 10^{-3} e$Å and $\mu_{step}^{F^-} = (5.8 \pm 0.5)\ 10^{-3} e$Å for stepped Au(001) in $SO_4^{2-}$, $ClO_4^-$ and $F^-$, respectively. These values are of comparable order of magnitude to what we find for Au kinks on (001) with co-adsorbed $Cl^-$ and $Br^-$, though slightly larger – in particular in the case of $Br^-$. This is reasonable since the adsorption site at a kink is electronically quite similar to step sites. Furthermore, the previous studies [13, 14] considered steps with an equilibrium concentration of kinks. Hence, the values previously reported for steps are not for entirely straight steps but include the contribution of the equilibrium number of kink sites.

Tansel and Magnussen recently published data on the dipole moment of hopping Cl adatoms adsorbed in surface sites on Cu(100) [10]. They find a dipole moment of $\mu_{Cu(100)}^{Cl} = 0.081\ e$Å, a value about an order of magnitude larger than our results for Au(001) kink sites with co-adsorbed chloride. The difference between our values for the kink dipole moments and their result for the dipole moment of a free surface adatom is reasonable. The charge redistribution is expected to be larger for freely migrating surface defects compared to step adatoms or kinks. Hence, the dipole moment for free defects should be larger than for strongly bound defects. A similar trend was found in embedded atom calculations for Ag(001) where the dipole moment increases when the number of broken bonds of a defect site increases[11].

The contribution of co-adsorbed halides to the kink dipole moment should be large. In general, co-adsorbed halide anions retain a small negative charge that reduces defect dipole moments: As was discussed in detail in [6], the work function of a surface is reduced when dipole moments are oriented with their positive end towards the electrolyte. This situation is found for defects such as adatoms, kinks, steps and adatom islands on metal surfaces. Partly negatively charged ad-ions reduce the dipole moment of a defect. This is in accordance with the observation of a lower adatom dipole moment of a chloride covered adatom on Cu(100) of $\mu_{Cu(100)}^{Cl} = 0.081\ e$Å [10] compared to $\mu_{Cu(100)} = 0.195\ e$Å for an adsorbate-free adatom on Cu(001) [6, 8]. We therefore expect that the dipole moments as found for kinks on Au(100) in chloride and bromide containing electrolytes are smaller than kink dipole moments in vacuum. Unfortunately, no further experimental or theoretical data on kink dipole moments exist to the best of our knowledge and cannot be compared here.

The various data available on dipole moments seem to follow a general trend: Free metal adatoms in an excited transition state are expected to have a considerably larger dipole moment than a defect in more strongly bound state or in the ground state. Here, more quantitative analyses would be of great help. In order to understand transport, migration and degradation processes on electrode materials in more detail in future more experimental and in particular theoretical data on defect dipole moments are desirable.

## Conclusions

We presented for the first time experimental data on the dipole moment of kinks under co-adsorption of $Cl^-$ and $Br^-$ by measuring the potential dependence of the kink energy and the surface charge. We find kink dipole moments, $\mu^{Cl} = (6.0 \pm 0.7) \times 10^{-3}\ e$Å and $\mu^{Br} = (10.1 \pm 0.6) \times 10^{-3}\ e$Å, respectively. Here the indices 'Cl' and 'Br' indicate that the kink dipole moment is that of an Au kink with co-adsorbed chloride and bromide rather than that of an uncovered Au kink atom.

As was previously demonstrated by our group [6, 7], defect dipole moments play a significant role in surface transport on metal electrodes in electrolyte. This is because defects with their associated dipole moment form and migrate within the strong electric field at the solid/liquid interface. Based on the method described here, one would be able to gather the dipole moment

of kink sites at steps for a large number of systems since the method is in principle applicable to all electrode-electrolyte systems. Therefore, the presented method could help to acquire quantitative information on migration phenomena at the solid/liquid interface.

## Acknowledgements

We acknowledge the skillful sample preparation by Udo Linke and Claudia Steufmehl ICS-7, FZ Jülich. Furthermore, we are grateful for helpful discussions with Wolfgang Schmickler, Ulm and Harald Ibach, PGI-3, FZ Jülich. Financial support provided by the Deutsche Forschungsgemeinschaft and by the Fond der Chemischen Industrie is greatly appreciated.

## Notes and references

[a] Institut für Elektrochemie, Universität Ulm, Albert-Einstein-Allee 47, 89069 Ulm, Germany.
[b] Institute of Complex Systems (ICS-7), Jülich Forschungszentrum GmbH, 52425 Jülich, Germany.
[c] Peter Grünberg Institute (PGI-6), Jülich Forschungszentrum GmbH, 52425 Jülich, Germany.
* Corresponding author; Email m.giesen@fz-juelich.de; Phone +49-2461-614524

1 M. Giesen, *Prog. Surf. Sci.*, 2001, **68**, 1.
2 M. R. Vogt, A. Lachenwitzer, O. M. Magnussen and R. J. Behm, *Surf. Sci.*, 1998, **399**, 49-69.
3 O. M. Magnussen and M. R. Vogt, *Phys. Rev. Lett.*, 2000, **84**, 357.
4 C. Punckt, M. A. Pope, J. Liu, Y. Lin and I. A. Aksay, *Electroanalysis*, 2010, **22**, 2834-2841.
5 M. S. Islam, D. J. Driscoll, C. A. J. Fisher and P. R. Slater, *Chemistry of Materials*, 2005, **17**, 5085-5092.
6 M. Giesen, G. Beltramo, S. Dieluweit, J. Muller, H. Ibach and W. Schmickler, *Surf. Sci.*, 2005, **595**, 127-137.
7 E. Pichardo-Pedrero, G. Beltramo and M. Giesen, *Appl. Phys.*, 2007, **A87**, 461 - 467.
8 J. E. Müller and H. Ibach, *Phys. Rev. B*, 2006, **74**, 085408.
9 N. Hirai, K. Watanabe and S. Hara, *Surf. Sci.*, 2001, **493**, 568.
10 T. Tansel and O. M. Magnussen, *Phys. Rev. Lett.*, 2006, **96**, 026101.
11 K. Pötting, N. B. Luque, P. M. Quaino, H. Ibach and W. Schmickler, *Electrochim. Acta*, 2009, **54**, 4494-4500.
12 E. Cockayne and B. P. Burton, *Phys. Rev. B*, 2004, **69**, 144116.
13 G. L. Beltramo, H. Ibach and M. Giesen, *Surf. Sci.*, 2007, **601**, 1876-1885.
14 G. L. Beltramo, H. Ibach, U. Linke and M. Giesen, *Electrochim. Acta*, 2008, **53**, 6818-6823.
15 Y.-C. Yang and O. M. Magnussen, *Phys. Chem. Chem. Phys.*, 2013, **15**, 12480-12487.
16 S. Baier and M. Giesen, *Phys. Chem. Chem. Phys.*, 2000, **2**, 3675.
17 M. Giesen and S. Baier, *J. Phys. Condens. Matter*, 2001, **13**, 5009.
18 D. M. Kolb, *Prog. Surf. Sci.*, 1996, **51**, 109-173.
19 H. Fink, x and Werner, *IBM Journal of Research and Development*, 1986, **30**, 460-465.
20 V. T. Binh, *Journal of Microscopy*, 1988, **152**, 355-361.
21 A. J. Melmed, *J Vac Sci Technol B*, 1991, **9**, 601-608.
22 M. Poensgen, J. F. Wolf, J. Frohn, M. Giesen and H. Ibach, *Surf. Sci.*, 1992, **274**, 430-440.
23 J. Clavilier, D. Armand, S. G. Sun and M. Petit, *J. Electroanal. Chem.*, 1986, **205**, 267-277.
24 A. Hamelin, *J. Electroanal. Chem.*, 1995, **386**, 1-10.
25 W. Schmickler, *Interfacial Electrochemistry*, Oxford University Press, New York, 1996.
26 G. Beltramo and E. Santos, *J. Electroanal. Chem.*, 2003, **556**, 127-136.
27 H.-C. Jeong and E. D. Williams, *Surf. Sci. Rep.*, 1999, **34**, 171.
28 M. Moiseeva, E. Pichardo-Pedrero, G. Beltramo, H. Ibach and M. Giesen, *Surf. Sci.*, 2009, **603**, 670-675.
29 G. Beltramo, M. Giesen and H. Ibach, *Electrochim. Acta*, 2009, **54**, 4305.
30 M. Giesen, J. Frohn, M. Poensgen, J. F. Wolf and H. Ibach, *J. Vac. Sci. Technol.*, 1992, **A10**, 2597.
31 J. F. Wolf, B. Vicenzi and H. Ibach, *Surf. Sci.*, 1991, **249**, 233.
32 S. Dieluweit, H. Ibach and M. Giesen, *Faraday Discuss.*, 2002, **121**, 27.
33 E. Pichardo-Pedrero and M. Giesen, *Electrochim. Acta*, 2007, **52**, 5659-5668.
34 S. Dieluweit and M. Giesen, *J. Electroanal. Chem.*, 2002, **524-525**, 194.
35 M. Giesen, C. Steimer and H. Ibach, *Surf. Sci.*, 2001, **471**, 80-100.
36 M. Giesen and D. M. Kolb, *Surf. Sci.*, 2000, **468**, 149-164.
37 P. Stoltze, *J. Phys. Condens. Matter*, 1994, **6**, 9495.



 